journal

J. Am. Ceram. Soc., 88 [11] 3192–3197 (2005)
DOI: 10.1111/j.1551-2916.2005.00584.x

High-Temperature Phase Equilibria of the Magnesium–Niobium–Titanate System

Robert I. Mangham*,† and William T. Petuskey*

Department of Chemistry, Arizona State University, Tempe, Arizona 85287

The high-temperature phase equilibria for the $MgO–Nb_2O_5–TiO_2$ system have been determined in air and at 1 atm O_2. Three isothermal sections, namely 1450°, 1350°, and 1250°C, were determined experimentally. From this, the 1000°C isothermal section was deduced by extrapolation. Throughout each diagram, most compounds were found to have an extended range of solubility, each exhibiting the same substitutional pattern of the combination $1/3(MgNb_2)^{4+}$ replacing Ti^{4+}. Furthermore, entropic stabilization because of cation mixing is evident for all phases except for the columbite solid solution, in which case the solid solution range decreased with increasing temperature.

I. Introduction

We have been studying phase equilibria in the quaternary system $PbO–MgO–Nb_2O_5–TiO_2$ at temperatures in the vicinity of 1000°C. A necessary first step has been the evaluation and refinement of the four ternary systems, of which we have already reported on the $PbO–MgO–Nb_2O$ equilibrium diagram.[1] Those of the $PbO–MgO–TiO_2$ and $PbO–Nb_2O_5–TiO_2$ systems will appear in other articles but are all ready presented in the form of a thesis.[2] We report here on the $MgO–Nb_2O_5–TiO_2$ system between 1000° and 1450°C at 1 atm. This includes not only mapping the phase compatibility relationships, but also an evaluation of the compositional limits of the compounds that exhibit significant solid solubility. Because of the limitations of slow diffusion, some aspects of the phase diagram at 1000°C were inferred by extrapolating data from higher temperature experiments (explained later).

The prime technological motivation for this work centers around the interest of reliably producing polycrystalline ceramics and large single crystals of ferroelectric relaxor compositions within the $Pb(Mg_{1/3}Nb_{2/3})O_3–PbTiO_3$ solid solution series. With respect to single crystals, the development of viable high-temperature methods by either solid state crystal growth[3] or flux growth methods[4] is hampered by a limited understanding of the phase equilibrium systems. While most current procedures have recognized the importance of maintaining slightly PbO- and MgO-rich environments to avoid the formation of the pyrochlore phases,[1] there is also a need to understand the chemistry of the PbO-poor side of the perovskite system in anticipation of the field advancing to the point where adjustments in the defect chemistry is needed to optimize physical properties. Consequently, the phase chemistry of the $MgO–Nb_2O_5–TiO_2$ system is a necessary component of that analysis.

Scientifically, the $MgO–Nb_2O_5–TiO_2$ system possesses interesting crystal chemistry because of the variety of phases that exist with octahedral sites for magnesium, niobium, and titanium. Wechsler *et al.*[5,6] have already pointed out that the three ternary compounds Mg_2TiO_4, $MgTiO_3$, and $MgTi_2O_5$ are entropically stabilized by the mixing of Mg^{2+} and Ti^{4+} on their respective lattice sites. Recognizing that the isovalent substitution of the $(Mg_{1/3}Nb_{2/3})^{4+}$ cation combination for Ti^{4+} characterizes the complete solubility range of the perovskite solid solution between $Pb(Mg_{1/3}Nb_{2/3})O_3$ (PMN) and $PbTiO_3$ (PT), it should therefore be expected that other compounds of the $MgO–Nb_2O_5–TiO_2$ system should also possess similar features. This has already been demonstrated for rutile where TiO_2 has been noted to dissolve up to 48 cation% of the formula unit $(Mg_{1/3}Nb_{2/3})O_2$ at 1000°C and 79 cation% at 1450°C.[7] We were interested in exploring the applicability of this same substitutional chemistry for the other structures of the system.

II. Experimental Procedure

(1) Sample Preparation

Prior to phase equilibrium measurements, batches of the binary oxides were prepared by reacting stoichiometric amounts of the constituent oxides. Rutile TiO_2 (Aldrich Chemical Co., 99.9% metals basis, <325 mesh), MgO (Alfa Aesar, 99.95% metals basis, <325 mesh), and niobium pentoxide Nb_2O_5 (Aldrich Chemical Co., 99.99% metal basis, <325 mesh) were dried at 120°C in a drying oven prior to use. Thermogravimetric analysis showed that only magnesium oxide retained small amounts of excess water under these conditions. This was taken into account for sample formulation. Grinding and mixing were typically carried out in an agate mortar and pestle or a plastic container with WC ball and end caps.

Pellets were made using a 1 cm steel hardened die with a Carver press (300–450 MPa). To eliminate any impurities scraped from the die walls, the outer edges of the pellets were lightly ground off using a diamond file. In general, the pellets were placed atop powder of the same composition inside platinum crucibles in a box furnace alongside a type-R thermocouple. Alumina crucibles were avoided because of reaction with niobium oxide. Phase purity and crystallinity were analyzed by powder X-ray diffraction (XRD).

The magnesium titanates were prepared from MgO and TiO_2. The samples were calcined for 20–40 h in air. The magnesium-rich Mg_2TiO_4 phase is borderline stable at 1000°C,[6] so the sample was prepared at higher temperatures (1050°–1100°C). The magnesium niobates $MgNb_2O_6$, $Mg_5Nb_4O_{15}$, and $Mg_4Nb_2O_9$ reported by Abbatista *et al.*[8] were prepared in a similar manner. The exception was that $Mg_5Nb_4O_{15}$ was annealed above 1250°C where it is stable. The niobium titanate phases were also prepared at 1000°C, and included $TiNb_2O_7$, $Ti_2Nb_{10}O_{29}$, and $TiNb_{24}O_{62}$.[9,10] Some discrepancies have been cited concerning the existence of a fourth phase, $TiNb_{14}O_{37}$, as to whether it is part of a solid solution extending from pure Nb_2O_5 or a stoichiometric compound. In this investigation, our interest lay elsewhere and did not focus on this region of the phase diagram.

R. S. Roth—contributing editor

Manuscript No. 20383. Received May 4, 2004; approved May 8, 2005.
This work was supported by the Air Force Office of Scientific Research under Grant No. AFOSR-ISSA-99-0031, which is administered through the Department of Commerce/NIST under Grant No. 60NANB000004/02.
*Member, American Ceramic Society.
†Author to whom correspondence should be addressed. e-mail: robmangham@yahoo.com

(2) Phase Equilibria Reactions

The main objective of this investigation was to determine the $MgO–Nb_2O_5–TiO_2$ phase diagram at 1000°C to complete the phase equilibria surrounding the PMN–PT solid solutions as stated in the introduction. However, samples prepared only at 1000°C did not develop sufficiently large grain size for microprobe analysis. Also, in most cases, because of sluggish diffusion, samples prepared at high temperatures (1350°C for example) and then further annealed at 1000°C for as much as 60 days, did not reach equilibrium at the lower temperature. This was evident by the presence of four phases when analyzed by microprobe and XRD. Therefore, three subsolidus, isothermal phase diagrams were determined separately at higher temperature anneals, from which the 1000°C compositions were extrapolated.

Using nearly 80 different compositions, combinations of the constituent binary oxides and/or pre-made ternary compounds were used to determine phase compatibilities which included determining the extent of solid solutions, and the compositional limits of two- and three-phase domains. Several pellets of each overall composition were formulated and individually annealed at separate isothermal temperatures, namely, 1450°C for 50 h and quenched, 1350°C for 75 h and quenched, 1250°C for 200 h and quenched and for some compositions at 1000°C for 600–900 h and quenched. Most samples were calcined in air; however, redundant samples prepared under flowing oxygen showed no difference in either phases present or solubility ranges. No investigation in oxygen stoichiometry was conducted. In cases where there was no melting, some anneals conducted at 1500°–1540°C for 3 h were included in this analysis. These higher temperatures (1250°C and above) were sufficient for grain growth as shown in the representative SEM (backscattered electron) image in Fig. 1. This figure corresponds to the three-phase equilibrium field *B* of a sample prepared from the constituent oxides and annealed at 1450°C for 50 h and then quenched. The dark gray phase is the rutile solid solution "TiO_2," the gray phase is the pseudobrookite solid solution "$MgTi_2O_5$," and the bright phase is the columbite solid solution "$MgNb_2O_6$." The relatively large grain size allowed easy composition analysis by electron microprobe.

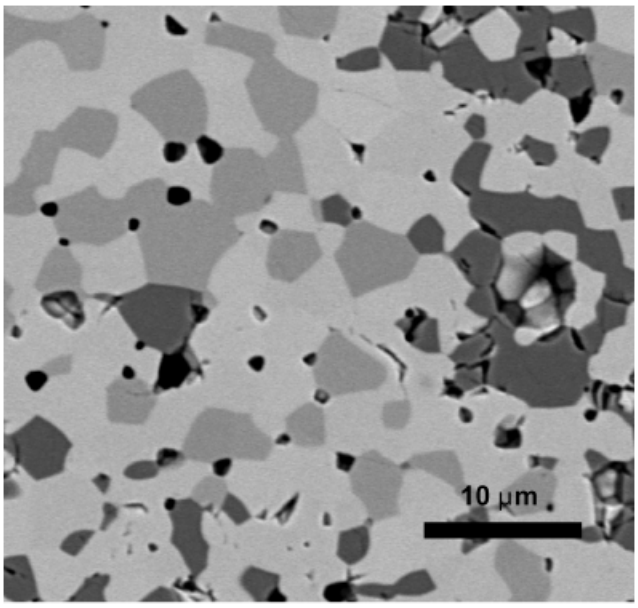

Fig. 1. Backscattered electron image of microstructures were analyzed for most equilibria conducted above about 1200°C. This figure corresponds to the three-phase equilibrium field *B* of a sample prepared from the constituent oxides and annealed at 1450°C for 50 h and then quenched. The dark gray phase is the rutile solid solution "TiO_2," the gray phase is the pseudobrookite solid solution "$MgTi_2O_5$," and the bright phase is the columbite solid solution "$MgNb_2O_6$." The relatively large grain size allowed easy composition analysis by electron microprobe. At lower temperatures, compositional limits were determined by peak shifts in X-ray diffraction patterns.

The different crystalline phases in each sample were analyzed by both powder XRD and electron microprobe wavelength dispersive spectroscopy (WDS). XRD data was collected on a Siemens D5000 diffractometer equipped with 7° wide position sensitive detector of Cu$K\alpha$ radiation. The compositional analyses were conducted using a JEOL 8600 electron microprobe with a takeoff angle of 40°. The samples were first imbedded in epoxy and polished down to 0.25 μm finish with diamond paste. No etchants were used. The samples were then coated with evaporated carbon ~150–200 Å. Composition standards for WDS were metallic niobium (Nb$L\alpha_1$) for niobium, rutile TiO_2 for titanium (Ti$K\alpha_1$), MgO for magnesium (Mg$K\alpha_1$), and Al_2O_3 for oxygen (O$K\alpha_1$). Standards were probed several times and calibration averaging was used. A focused 2 μm beam running at 10 nA and 15 KeV accelerated voltage was used. Grains typically on the order of 20–40 μm or more were easily analyzed by the electron microprobe. The accuracy of the measured compositions was assessed using compounds of this system, like $MgTiO_3$, that have well-established stoichiometries. Agreement was considered good when errors were within ± about 1/2 cation%.

III. Results and Discussion

The subsolidus phase diagrams for the $MgO–Nb_2O_5–TiO_2$ system are presented for 1450°, 1350°, 1250°, and 1000°C as shown in Figs. 2, 3, 4, and 5, respectively. The phase compositions for the various equilibria are given in Tables I–VII. The main feature for each diagram is the extent of the various solid solutions. These results complement the XRD analysis by Relando *et al.*[11] Their investigation reports solid solutions between the columbite-rutile, pseudobrookite, and ilmenite-corundum binaries at 1100° and 1250°C. The niobium-rich region on this isothermal section has been omitted as our data was inconclusive concerning the extent of the liquid regions extending from both the $Nb_2O_5–TiO_2$ and $Nb_2O_5–MgO$ binary joins. However, phase field *G* (not shown in the 1450°C ternary) at 1400°C reveals ~3.5 cation% Mg^{2+} in $TiNb_2O_7$ and ~2.8 cation% in $Ti_2Nb_{10}O_{29}$ (see Table VI) in equilibration with rutile.

The composition range of rutile (TiO_2) solid solution extended from pure TiO_2 to about 79 cation% substitution of $(Mg_{1/3}Nb_{2/3})^{4+}$ for Ti^{4+} at 1450°C, and to 47% at 1000°C as extrapolated from higher temperatures (our procedure is explained later). This is in excellent agreement with Baumgarte and Blachnik's[7] work who found 79% (±2 mol%) and 48%, for

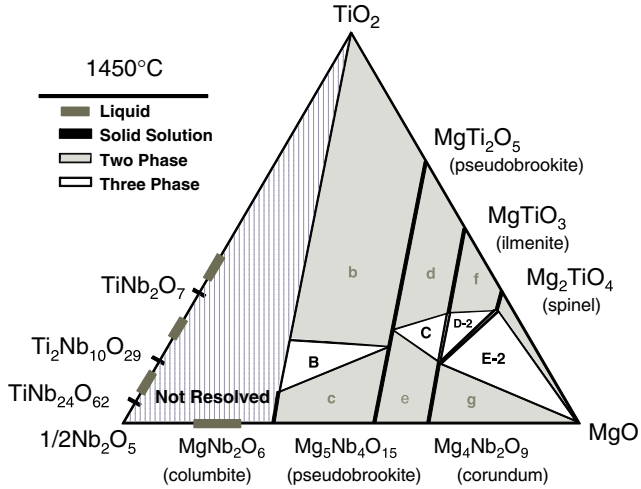

Fig. 2. Phase equilibrium diagram for the $MgO–Nb_2O_5–TiO_2$ system at 1450°C and 1 atm. Solid solutions are shown in black, two-phase domains in gray, and the three-phase domains in white. Compositional limits for the phase fields were determined by electron microprobe analysis wavelength dispersive spectroscopy and the values are presented in Tables I–VII.

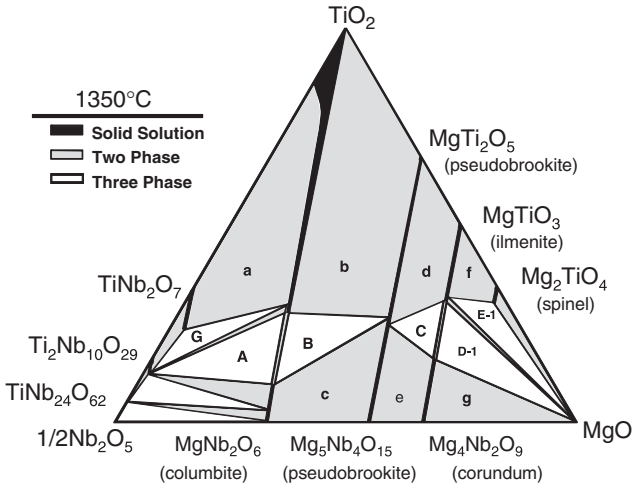

Fig. 3. Phase equilibrium diagram for the $MgO–Nb_2O_5–TiO_2$ system at 1350°C and 1 atm. Solid solutions are shown in black, two-phase domains in gray, and the three-phase domains in white. With respect to the higher temperature diagram (1450°C) the phase fields *A*, *B*, and *C* have increased in range. The thermal compatibility between the $Mg_4Nb_2O_9$ and Mg_2TiO_4 phase no longer exists as the $MgTiO_3$ solid solution is now in thermal equilibrium with the MgO phase.

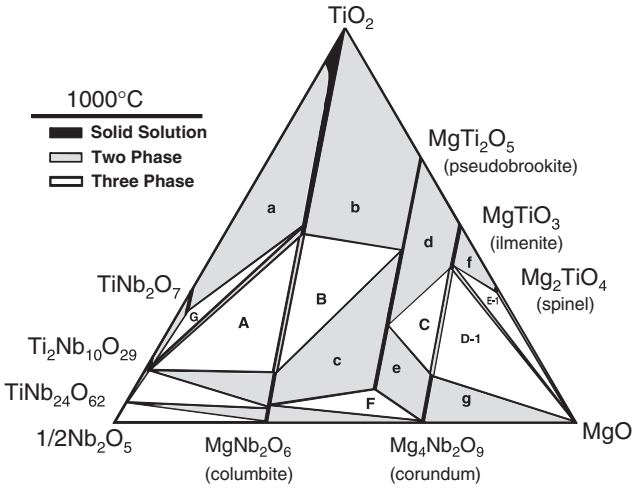

Fig. 5. Extrapolated phase equilibrium diagram for the $MgO–Nb_2O_5–TiO_2$ system at 1000°C and 1 atm. A series of solid solutions are shown in black, while the two-phase regions are shown in gray, and three-phase domains in white. The compositions limits in phase field *A*, *B*, *C*, *D-1*, and *E-1* were calculated from the higher temperature phase equilibrium diagrams at 1450°, 1350°, and 1250°C (see Figs. 2–4).

the same temperatures. The solubility limit was measured for both niobia-rich side and magnesia-rich field *B* equilibria. These values were within 1 cation% (see Tables I and II), reflecting on the narrowness of the composition range perpendicular to the $(Mg_{1/3}Nb_{2/3})^{4+}–Ti^{4+}$ substitution scheme. Columbite ($MgNb_2O_6$), which is structurally related to rutile, exhibits a small solubility range for TiO_2. At 1450°C, it contains up to 8 cation% Ti^{4+}, and increases with decreasing temperature to 13 cation%, at 1000°C.

The ternary phase field *B* corresponds to rutile and columbite solid solutions equilibrating with the pseudobrookite ($Mg_5Nb_4O_{15}–MgTi_2O_5$) solid solution. This was measured directly at 1450°, 1350°, and 1250°C. The Ti^{4+} composition ranged from 20.6 cation% at 1450°C to 43.1% at 1000°C. The composition of the pseudobrookite phase shifted to the titania-rich region with decreasing temperature. This trend is consistent with the thermal instability of the titania-free $Mg_5Nb_4O_{15}$ phase below 1250°C.

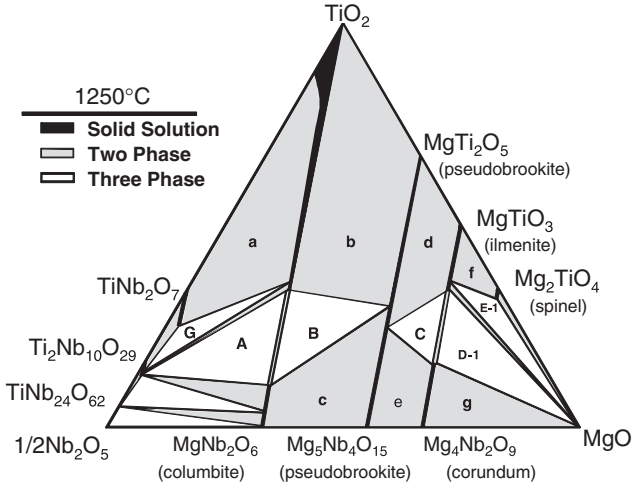

Fig. 4. Phase equilibrium diagram for the $MgO–Nb_2O_5–TiO_2$ system at 1250°C and 1 atm. Solid solutions are shown in black, two-phase domains in gray, and the three-phase domains in white. Phase fields *A*, *B*, and *C* have increased in range with respect to the higher temperature diagrams 1450°C and 1350°C, and phase field *D-1* has also increased in range with respect to the diagram at 1350°C.

Phase field *C* corresponds to the pseudobrookite solid solution equilibrating with the corundum ($Mg_4Nb_2O_9$) and ilmenite ($MgTiO_3$) solid solutions. This field was also evaluated at 1500°C. The compositions are given in Table III. The pseudobrookite solid solution is dramatically less temperature sensitive in phase field *C* then in field *B*. In field *C*, the Ti^{4+} content was essentially constant from 1450° to 1250°C, whereas in field *B*, it increased with decreasing temperature by as much as 10 cation% for the same temperature range.

As titania-free $Mg_5Nb_4O_{15}$ does not exist below 1250°C, the 1000°C section forms a new ternary equilibrium between the pseudobrookite solution with the columbite and corundum solid solutions (labeled *F*). Although XRD confirmed the result, because of the small grain size for samples prepared at 1000°C compositional data was not measured directly. From the surrounding phase equilibrium fields *A*, *B*, and *C*, we estimate the columbite phase to contain as much as 5 cation% Ti^{4+}. The extrapolated composition at 1000°C for the pseudobrookite solid solution is 8 cation% Ti^{4+}.

The extent of the ilmenite ($MgTiO_3$) solid solution was directly measured to contain nearly 16 cation% Nb^{5+} at 1450°C, which decreased with decreasing temperature. Eight cation% Nb^{5+} solubility at 1000°C was estimated by extrapolation. The ilmenite composition was also independently measured at each isotherm in the three-phase fields *C*, and *D-2*/*D-1*.

The corundum solid solution ($Mg_4Nb_2O_9$), at the bottom of the $Mg_4Nb_2O_9–MgTiO_3$ tie line, also exhibits significant

Table I. Cation Composition for Phase Field *A*

Temperature (°C)/time (h)	Phase	% cation composition† Mg	Nb	Ti
1250/200	$Ti_2Nb_{10}O_{29}$	0.9 (02)‡	84.4 (2)	14.7 (3)
	$MgNbO_6$	29.4 (2)	60.1 (3)	10.5 (1)
	Rutile	21.9 (4)	45.7 (1)	32.4 (4)
1350/100	$Ti_2Nb_{10}O_{29}$	1.3 (1)	85.1 (3)	13.6 (2)
	$MgNbO_6$	30.0 (2)	60.6 (1)	9.3 (05)
	Rutile	23.9 (04)	49.5 (2)	26.5 (2)
1400/60	$Ti_2Nb_{10}O_{29}$	1.5 (02)	86.5 (02)	11.9 (1)
	$MgNbO_6$	30.4 (1)	61.4 (2)	8.7 (07)
	Rutile	24.6 (1)	52.1 (2)	23.3 (2)

†Determined by electron microprobe wavelength dispersive spectroscopy (WDS). ‡"( )" refers to standard deviations.

Table II. Cation Composition for Phase Field *B*

Temp (°C)/time (h)	Phase	% cation composition† Mg	Nb	Ti
1250/200	Rutile	22.3 (08)‡	44.7 (2)	33.1 (06)
	$MgTi_2O_5$	44.9 (1)	24.4 (2)	30.6 (1)
	$MgNb_2O_6$	29.4 (3)	59.8 (1)	10.7 (07)
1350/100	Rutile	24.1 (2)	48.7 (2)	27.2 (09)
	$MgTi_2O_5$	46.7 (02)	27.7 (04)	25.6 (01)
	$MgNb_2O_6$	29.7 (2)	60.4 (2)	9.9 (04)
1450/50	Rutile	26.0 (3)	52.3 (5)	21.7 (2)
	$MgTi_2O_5$	48.3 (1)	31.1 (2)	20.6 (1)
	$MgNb_2O_6$	30.6 (3)	60.9 (2)	8.6 (07)

†Determined by electron microprobe wavelength dispersive spectroscopy (WDS). ‡"( )" refers to standard deviations.

Table III. Cation Composition for Phase Field *C*

Temp (°C)/time (h)	Phase	% cation composition† Mg	Nb	Ti
1250/200	$MgTi_2O_5$	46.6 (4)‡	29.0 (3)	24.4 (3)
	$MgTiO_3$	54.7 (2)	12.4 (2)	32.7 (2)
	$Mg_4Nb_2O_9$	60.6 (4)	24.2 (2)	15.2 (5)
1350/100	$MgTi_2O_5$	46.9 (08)	28.6 (2)	24.5 (1)
	$MgTiO_3$	55.5 (3)	13.6 (9)	30.9 (12)
	$Mg_4Nb_2O_9$	60.1 (3)	25.3 (3)	16.6 (2)
1450/50	$MgTi_2O_5$	46.8 (5)	28.7 (4)	24.5 (07)
	$MgTiO_3$	56.3 (5)	15.8 (06)	28.0 (5)
	$Mg_4Nb_2O_9$	60.0 (2)	23.3 (08)	16.7 (2)
1500/3	$MgTi_2O_5$	46.3 (1)	26.7 (08)	26.0 (1)
	$MgTiO_3$	52.2 (1)	15.7 (06)	29.0 (08)
	$Mg_4Nb_2O_9$	59.1 (08)	22.5 (07)	18.4 (06)

†Determined by electron microprobe wavelength dispersive spectroscopy (WDS). ‡"( )" refers to standard deviations.

dissolution of titanium. At 1500°C, corundum dissolves up to 18.5 cation% Ti^{4+}, and decreased with decreasing temperature to the extrapolated value of 12 cation% at 1000°C. The measured compositional values were consistent within 1 cation% for phase fields, *C*, *D-1*, *D-2*, and *E-2* at each isothermal section.

Between 1400° and 1350°C, the compatibility between corundum and the inverse spinel becomes thermodynamically unstable, forming a new binary compatibility between ilmenite and pure MgO. The corundum solid solution below 1400°C continues to equilibrate with the ilmenite solid solution and MgO forming the phase field labeled *D-1*. However, the new binary join between the ilmenite solid solution and MgO isolates the inverse spinel phase, thus confining it to the ternary field labeled *E-1*.

Table IV. Cation Composition for Phase Fields *D-1* and *E-1*

Temp (°C)/time (h)	Phase	% cation composition† Mg	Nb	Ti
1150/400	$MgTiO_3$	53.1 (12)‡	7.0 (22)	39.9 (34)
	$Mg_4Nb_2O_9$	66.21 (3)	24.3 (4)	13.6 (3)
	MgO	100		
1250/200	$MgTiO_3$	54.7 (1)	12.4 (2)	32.9 (08)
	$Mg_4Nb_2O_9$	59.9 (2)	23.7 (1)	16.3 (1)
	MgO	100		
1350/100	$MgTiO_3$	56.1 (3)	13.6 (2)	30.2 (08)
	$Mg_4Nb_2O_9$	61.0 (4)	22.4 (3)	16.5 (2)
	MgO	100		
1250/200	$MgTiO_3$	54.0 (1)	9.7 (2)	36.3 (2)
	Mg_2TiO_4	67.0 (3)	1.9 (06)	31.1 (3)
	MgO	100		
1350/100	$MgTiO_3$	55.7 (2)	13.3 (08)	31.0 (1)
	Mg_2TiO_4	67.3 (09)	2.7 (1)	29.8 (2)
	MgO	100		

†Determined by electron microprobe wavelength dispersive spectroscopy (WDS). ‡"( )" refers to standard deviations.

Table V. Cation Composition for Phase Fields *D-2* and *E-2*

Temp (°C)/time (h)	Phase	% cation composition† Mg	Nb	Ti
1400/60	$MgTiO_3$	55.6 (2)‡	14.7 (1)	29.6 (3)
	Mg_2TiO_4	66.9 (5)	3.3 (2)	29.7 (2)
	$Mg_4Nb_2O_9$	59.6 (1)	23.3 (2)	17.0 (4)
1450/50	$MgTiO_3$	57.2 (1)	13.8 (1)	29.0 (4)
	Mg_2TiO_4	66.2 (3)	3.7 (2)	30.1 (3)
	$Mg_4Nb_2O_9$	58.8 (1)	23.3 (2)	17.8 (2)
1400/60	Mg_2TiO_4	67.4 (3)	3.3 (2)	29.1 (2)
	$Mg_4Nb_2O_9$	59.7 (2)	23.4 (1)	16.8 (0)
	MgO	100		
1450/50	Mg_2TiO_4	67.5 (2)	3.6 (08)	28.9 (2)
	$Mg_4Nb_2O_9$	60.2 (07)	23.2 (1)	16.6 (1)
	MgO	100		
1450/30	Mg_2TiO_4	67.6 (05)	3.6 (07)	28.8 (1)
	$Mg_4Nb_2O_9$	60.6 (2)	22.8 (1)	16.5 (06)
	MgO	100		

†Determined by electron microprobe wavelength dispersive spectroscopy (WDS). ‡"( )" refers to standard deviations.

All of the two-phase domains were evaluated by XRD, and several of the high-temperature samples were also analyzed by electron microprobe. Among these are the phase fields *b*, *c*, *d*, *e*, and *f*. Table VII shows the overall and equilibrium phase compositions. The width of the binary phase field *j* was estimated from the boundaries in ternary phase field *A* and from lower temperature studies in this investigation. The existence of the binary join between $TiNb_{24}O_{62}$ and $MgNb_2O_6$ was established by X-ray powder diffraction. No further investigation was conducted on the Nb_2O_5-rich side of $TiNb_{24}O_{62}$.

The solubility of Nb_2O_5 in rutile (TiO_2) was analyzed on a sample prepared with an overall content of 10 cation% Nb^{5+} with TiO_2. At 1450°C, all of the niobium dissolved as was evident by the absence of $TiNb_2O_7$. A sample prepared at 1000°C and 400 h dissolved ~4.5 cation% Nb^{5+} in the rutile structure with the balance of the Nb_2O_5 appearing in $TiNb_2O_7$. This was in agreement with the results reported by Dirstine and Rosa.[12]

The solubility of Mg^{2+} in TiO_2 rutile was measured at 1350° and 1250°C. No detection of dissolved MgO was found in the rutile phase as determined by microprobe analysis. Instead, all of the MgO reacted with excess rutile to form the pseudobrookite phase $MgTi_2O_5$. Therefore we concluded there is no discernable dissolution of Mg^{2+} in rutile at 1000°C.

In most cases, the extent of the solid solution in this system could be monitored by the shifting of diffraction peaks solely in XRD patterns. A prime example is the rutile and columbite solid solutions binary join (Fig. 6). An expansion around the (110) reflection for rutile is shown at left (a). The peak at 27.5° 2θ

Table VI. Cation Composition for Phase Field *G*

Temp (°C)/time (h)	Phase	% cation composition† Mg	Nb	Ti
1400/50	$TiNb_2O_7$	3.4 (09)‡	74.2 (3)	22.2 (2)
	$Ti_2Nb_{10}O_{29}$	1.0 (2)	84.2 (1)	14.8 (06)
	Rutile	21.3 (08)	45.4 (1)	33.2 (2)

†Determined by electron microprobe wavelength dispersive spectroscopy (WDS). ‡"( )" refers to standard deviations.

Table VII. Cation Compositions for Various Binary Phase Fields

	Starting composition cation%					% cation composition		
Phase field	Mg	Nb	Ti	Temp/time (°C)/(h)	Phase	Mg	Nb	Ti
b	30.0	20.0	50.0	1400/10	Rutile	10.7 (08)‡	21.7 (1)	67.6 (2)
				+1000/560	$MgTi_2O_5$	37.2 (1)	8.5 (3)	54.3 (1)
b	2.0	3.0	95.0	1400/50	Rutile	10.7 (08)	21.7 (1)	67.6 (2)
				+1200/65	$MgTi_2O_5$	37.2 (1)	8.5 (3)	54.3 (1)
				+1000/1100				
				1400/50	Rutile	10.7 (1)	21.9 (4)	67.3 (3)
				+1200/65	$MgTi_2O_5$	37.2 (09)	8.3 (4)	54.3 (1)
				1400/50	Rutile	10.7 (1)	21.7 (1)	67.6 (1)
					$MgTi_2O_5$	37.2 (09)	8.4 (2)	54.4 (3)
c	53.0	42.5	4.5	1400/12	$MgNb_2O_6$	32.2 (2)	66.9 (1)	0.8 (07)
					$MgTi_2O_5$	53.1 (3)	41.5 (7)	5.4 (3)
c	42.5	42.5	15.0	1400/16	$MgNb_2O_6$	30.1 (2)	62.0 (3)	7.8 (2)
				+1000/650	$MgTi_2O_5$	47.1 (6)	30.6 (2)	22.4 (1)
				1400/16	$MgNb_2O_6$	30.5 (3)	61.7 (3)	8.2 (4)
					$MgTi_2O_5$	47.0 (2)	30.3 (09)	22.7 (1)
d	45.0	5.0	50.0	1400/10	$MgTi_2O_5$	36.6 (4)	7.7 (2)	55.7 (3)
				+1000/560	$MgTiO_3$	49.5 (2)	2.2 (1)	48.1 (3)
e	58.0	30.0	12.0	1400/16	$Mg_4Nb_2O_9$	62.5 (1)	27.9 (09)	9.6 (3)
				+1000/650	$MgTi_2O_5$	48.3 (1)	33.4 (2)	18.3 (1)
				1400/16	$Mg_4Nb_2O_9$	62.0 (7)	28.1 (3)	9.9 (3)
					$MgTi_2O_5$	48.5 (4)	32.7 (2)	18.8 (1)
f	64.0	32.0	4.0	1000/200	$MgTiO_3$	54.6 (8)	5.1 (14)	40.2 (26)
					Mg_2TiO_4	63.4 (12)	.7 (4)	35.9 (26)
				1400/20	$MgTiO_3$	54.8 (1)	11.0 (1)	34.3 (07)
				+1250/50	Mg_2TiO_4	66.9 (2)	2.1 (1)	31.1 (08)
				1400/20	$MgTiO_3$	54.6 (03)	11.2 (07)	34.2 (06)
					Mg_2TiO_4	66.8 (1)	2.3 (2)	31.0 (08)

†Determined by electron microprobe wavelength dispersive spectroscopy (WDS). ‡"( )" refers to standard deviations.

corresponds to phase pure TiO_2, while the three peaks to the left indicate an increasing lattice parameter with increasing concentrations. Generally, rutile dissolved more $(Mg_{1/3}Nb_{2/3})^{4+}$ with increasing temperature. Although less dramatic, columbite also exhibits peak shifting because of TiO_2 dissolution (Fig. 6). As pointed out previously, the columbite phase exsolves Ti^{4+} with increasing temperature. Therefore, the columbite diffraction lines shifted to lower 2θ values consistent with an expanding lattice parameter. The same diffraction peaks (rutile (110), and columbite (131)) were extrapolated to 1000°C to compare with the microprobe analysis in determining solid solution compositions. Good agreement (less than 1 cation% deviation) for extrapolated values at 1000°C between XRD and microprobe analysis was observed. The X-ray data gave 13.5 and 47.2 cation% Ti^{4+} for columbite and rutile solid solutions, and the WDS data gave 14.1 and 47.2 cation%, respectively.

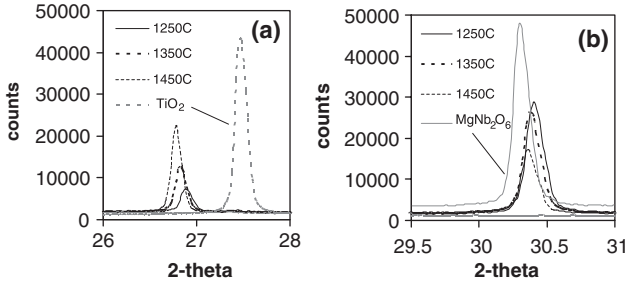

Fig. 6. Selected X-ray diffraction peaks for rutile and columbite solid solutions along their common binary join at various temperatures. The (110) rutile diffraction line is shown at left (a). The amount of this phase increases with temperature as well as shifts to smaller 2θ. The peak at right (b) is the (131) reflection for the columbite solid solution. The amount of this phase decreases with temperature, and the peaks shift to lower 2θ (increasing *d*-spacing). This corresponds to a decrease in Ti^{4+} content with increasing temperature.

As already stated, the compositional limits for the three-phase equilibrium domains at 1000°C were extrapolated from higher temperature data. The plots in Figs. 7 and 8 are for the various solid solutions of this system as a function of temperature. Figure 7 shows the columbite and rutile solid solutions. Two sets of data are shown, corresponding to measurements collected from the three phase fields *A* and *B*. Generally, a linear relationship is well defined between solubility and temperature.

Likewise, Fig. 8 shows the solubility limit of ilmenite and corundum as a function of temperature. Again two sets of data appear corresponding to phase fields *C* and *D-1*. The solubilities

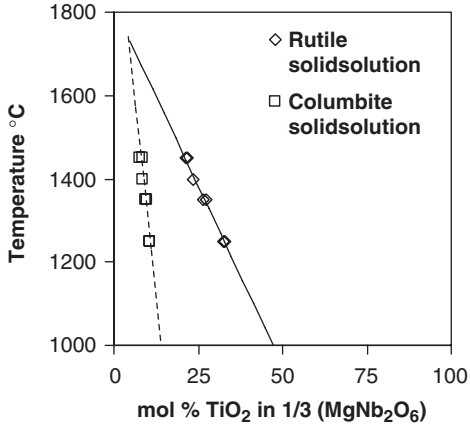

Fig. 7. Plot of rutile and columbite solid solution compositions versus temperature. The two data sets were acquired from phase field *A* and *B* using wavelength dispersive spectroscopy microprobe analysis (see Tables I and II). Extrapolated values at 1000°C for rutile and columbite solid solutions are 47.2 mol% TiO_2 (47.2 cation% Ti^{4+}) in 1/3($MgNb_2O_6$) and 14.1 mol% TiO_2 (14.1 cation% Ti^{4+}) in 1/3($MgNb_2O_6$), respectively.

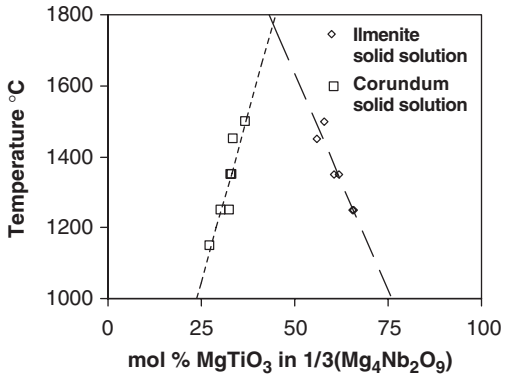

Fig. 8. Plot of the ilmenite and corundum solid solution compositions versus temperature. The data points were acquired from electron microprobe wavelength dispersive spectroscopy analysis from phase field *C* and *D-1*. Extrapolated values at 1000°C for ilmenite and corundum solid solutions are 75.9 mol% (38.0 cation%) and 23.7 mol% (11.8 cation% Ti^{4+}), respectively.

Table VIII. Calculated Cation Compositions at 1000°C in the $MgO–Nb_2O_5–TiO_2$ System

	% cation composition		
Phase	Mg	Nb	Ti
$Ti_2Nb_{10}O_{29}$	1	84	15
Rutile ss	18	35	47
Columbite ss	29	58	13
Pseudobrookite ss (⊘ *F*)	53	39	8
Pseudobrookite ss (⊘ *B*)	41	16	43
Pseudobrookite ss (⊘ *C*)	47	29	24
Ilmenite ss	54	8	38
Corundum ss	62	26	12
Inverse spinel ss	~66	<1	~33

ss, solid solution.

extrapolated to 1000°C are 38.0 for ilmenite and 11.8 cation% Ti^{4+} for corundum. Table VIII list the extrapolated values for each of the solid solutions at 1000°C.

IV. Conclusion

Four isothermal sections of the $MgO–Nb_2O_5–TiO_2$ phase diagram were analyzed and presented. The phase equilibria at 1450°, 1350°, and 1250°C were experimentally determined, whereas the 1000°C diagram was deduced by extrapolation from the higher temperature diagrams. Many compounds were found to have an extended range of solubility each exhibiting the same substitutional pattern of the combination $1/3(MgNb_2)^{4+}$ replacing Ti^{4+}. TiO_2 and the magnesium titanates displayed the largest accommodation for the solute cations, Mg^{2+} and Nb^{5+}. In the rutile (TiO_2) phase, up to 79 cation% of Ti^{4+} was replaced. Other structures exhibiting the same substitutional scheme were pseudobrookite $Mg(Ti,Mg,Nb)_2O_5$, ilmenite $Mg(Ti,Mg,Nb)O_3$, corundum $Mg_4(Ti,Mg,Nb)_2O_9$, and to a much lesser extent, spinel $Mg_2(Ti,Mg,Nb)O_4$.

Entropic stabilization because of cation mixing is evident for all phases except for the columbite solid solution. In the latter case the solid solution range decreased with increasing temperature. In addition, pseudobrookite exists in three ternary phase fields (*B*, *C*, and *F*) at 1000°C. However, contrary to the other solid solutions in this system, when pseudobrookite equilibrates with ilmenite and corundum (phase field *C* 1250°–1450°C) the composition remains independent of temperature. The relatively similar bond lengths for the cations in the octahedral position (Mg–O = 2.099 Å, Nb–O = 1.978 Å, Ti–O = 1.965 Å), results in small volume changes in lattice parameters by way of cation mixing along the solid solutions. Although in some cases these volume changes are significant enough to detect by XRD, none the less the volume change is sustainable to a significant degree of substitution.

References

[1]P. Lucas and W. T. Petuskey, "Phase Equilibria in the Lead–Magnesium–Niobium–Oxygen System at 1000°C," *J. Am. Ceram. Soc.*, **84** [9] 2150–2 (2001).
[2]R. I. Mangham, Ph.D. Degree in Chemistry, Arizona State University, Tempe, AZ, 2003.
[3]S. L. Swartz, T. R. Shrout, W. A. Schulze, and L. E. Cross, "Dielectric Properties of Lead–Magnesium Niobate Ceramics," *J. Am. Ceram. Soc.*, **67** [5] 311–5 (1984).
[4]J. P. Guha, D. J. Hong, and H. A. Anderson, "Effects of Excess PbO on the Sintering and Dielectric Properties of $Pb(Mg_{1/3}Nb_{2/3})O_3–PbTiO_3$-Based Ceramics," *J. Am. Ceram. Soc.*, **71** [3] C-152–4 (1988).
[5]B. A. Wechsler and R. B. Von Dreele, "Structure Refinements of Mg_2TiO_4, $MgTiO_3$ and $MgTi_2O_5$ by Time-of-Flight Neutron Powder Diffraction," *Acta Crystallogr.*, **B45**, 542–9 (1989).
[6]B. A. Wechsler and A. Navrotsky, "Thermodynamics and structural Chemistry of Compounds in the System $MgO–TiO_2$," *J. Solid State Chem.*, **55**, 165–80 (1984).
[7]A. Baumgarte and R. Blachnik, "New M^{2+} M^{4+} Nb_2O_8 Phases," *J. Alloys Compd.*, **215**, 117–20 (1994).
[8]F. Abbatista, P. Rolando, and G. Borroni Gassi, "Sol Sistema $MgO–Nb_2O_5$," *Ann. Chim. (Rome)*, **60**, 426–35 (1970).
[9]R. S. Roth and L. W. Coughanour, "Phase-Equilibrium Relations in the Systems Titania–Niobia and Zirconia–Niobia," *J. Res. Nat. Bur. Stand.*, **55** [4] 209 (1955).
[10]N. F. Fedorov *et al.*, "The $Nb_2O_5–TiO_2$ System," *Russ. J. Inorg. Chem.*, **34** [5] 1316–9 (1989).
[11]P. Relando *et al.*, "Study of the Magnesium Oxide–Niobium Oxide (Nb_2O_5)–Titanium (IV) Oxide System," *Atti Accad. Sci. Torino*, **10** [1] 113–24 (1976) (written in Italian).
[12]R. T. Dirstine and C. J. Rosa, "Defect Structure and Related Thermodynamic Properties of Nonstoichiometric Rutile (TiO_{2-x}) and Nb_2O_5 Doped Rutile," *Z. Metallkund.*, **70** [6] 372–8 (1979). □